MOLEKUL
eISSN: 2503-0310

Articles
https://doi.org/10.20884/1.jm.2024.19.3.11001

Molecular Vibration and Physicochemical Performance of Proton-Conducting Solid Polymer Electrolyte Membrane based on CMC/PVA/CH_3COONH_4

Sun Theo Constan Lotebulo Ndruru[1]*, Elvira Nur Rachmadhanti[2], Shanny Fridarima[2], Nila Tanyela Berghuis[2], Ridho Prasetyo[3], Evi Yulianti[4], Atika Trisna Hayati[1], Risda Adriana[5], Rabiyatul Adawiyah Siregar[6], Muhammad Ihsan Sofyan[1], Yulianti Sampora[1], Dicky Annas[1], Mohammad Jihad Madiabu[7]

[1]Research Center for Chemistry, National Research and Innovation Agency (BRIN) RI, Kawasan Saintek B.J. Habibie, Tangerang Selatan, Indonesia
[2]Chemistry Department, Faculty of Sciences and Computer Science, Pertamina University, Jakarta Selatan, Indonesia
[3]Chemical Engineering Department, Universitas Diponegoro, Semarang, Indonesia
[4]Research Center for Advanced Chemistry National Research and Innovation Agency (BRIN) RI, Kawasan Saintek B.J. Habibie, Tangerang Selatan, Indonesia
[5]Chemistry Department, Universitas Hasanuddin, Makassar, Indonesia
[6]Education Doctoral Program, Universitas Lampung, Bandar Lampung, Indonesia
[7]Department of Analytical Chemistry, Politeknik AKA Bogor, Bogor, Indonesia

*Corresponding author email: sunt002@brin.go.id

Received January 15, 2024; **Accepted** October 03, 2024; **Available online** November 20, 2024

ABSTRACT. This work examined the influence of ammonium acetate (CH_3COONH_4) on CMC/PVA-based solid polymer electrolyte (SPE) membranes, focusing on molecular vibration, proton conductivity, and physicochemical properties. SPE membranes were prepared via the casting solution method with varying CH_3COONH_4 concentrations to determine the optimal proton conductivity. Various characterizations, including FTIR, EIS, XRD, and TGA, were performed. The optimal membrane condition was achieved with 10 wt-% CH_3COONH_4 in the CMC/PVA (80/20) blend, yielding proton conductivity of 3.93×10^{-4} S/cm and favorable mechanical, thermal, and crystallinity properties, making it suitable for proton-conducting polymer applications.

Keywords: ammonium acetate, carboxymethyl cellulose, ionic conductivity, poly(vinyl alcohol), proton battery, solid electrolyte membrane.

INTRODUCTION

Solid polymer electrolyte (SPE) membrane is a crucial component in developing energy storage and energy supply such as fuel cells, dye-sensitized solar cells (DC), supercapacitors (SC) and secondary batteries (Di Noto et al., 2011). All-solid-state secondary batteries, especially, SPE membranes have dual functions, including electrode compartment separators and also as electrolytes (Lizundia & Kundu, 2021). Proton batteries are a type of alternative battery that can replace metal-based or metal-ion-based batteries that have been developed so far, such as lithium-ion batteries, sodium-ion batteries, magnesium-ion batteries, zinc-ion batteries, and others (Lizundia & Kundu, 2021). Proton batteries generally utilize protons as charge carriers moving from the anode to the cathode and vice versa. Similar to solid-state metal ion secondary batteries, solid polymer electrolytes are crucial for enhancing the performance of these devices (Li et al., 2021).

The selection of the type of polymer to serve as the host for proton conduction is crucial in the development of the SPE membrane (Hoang Huy et al., 2021a; Nagao, 2024). It is well known that the primary drawback of SPEs is their very low ionic conductivity (Ngai et al., 2016), if it is compared to the liquid electrolyte (Hoang Huy et al., 2021b). Flexible and stable thermal SPE membrane behaviour is preferred because it offers its safety (Fu et al., 2019) over liquid electrolytes that have low vapour points, flammable and corrosive (Zulkifli et al., 2020). Nevertheless, to realize a physically stable and high electrical conductivity SPE membrane is challenging.

Several studies on SPEs for proton batteries, also known as proton-conducting polymers, generally utilize commercially available synthetic polymers such as polyethylene oxide (PEO)(Borodin & Smith, 2006),

polyacrylonitrile (PAN)(Yang et al., 2017), polyvinylidene fluoride (PVDF) (Zhang et al., 2017), poly(propylene carbonate)(PPC) (Zhang et al., 2015), etc. However, the use of these synthetic polymers poses environmental concerns when developed on a large scale, as they are not biodegradable (Xi et al., 2021). Therefore, there is a significant shift towards using environmentally friendly polymers as hosts for polymer electrolytes in proton batteries. These eco-friendly polymers are typically derived from biomass, such as carboxymethyl cellulose (CMC).

CMC is a significant cellulose derivative, alongside methylcellulose (MC) and cellulose acetate (CA). CMC exhibits several advantageous physical properties: it is easily soluble in water, mixes well with various salts, is thermally and mechanically stable, and is biodegradable in nature (Xi et al., 2021). Besides its good physical properties, CMC also has a stable molecular structure with β-(1,4) bonds between its glucose monomer units, similar to cellulose (Ndruru, Asta, et al., 2024). The various functional groups in CMC molecules, such as O-H, C=O, O=C-OH, and C-OH, provide multiple sites for the transit of charge-carrying ions, facilitating their movement from one site to another(Akhlaq et al., 2023). It's same cases with the single host polymers in SPEs, CMC also requires supporting materials to enhance the segmental motion of its polymer chains, thereby contributing to increased (ion/proton) conductivity (Ndruru et al., 2024).

The blending technique is the easiest and most cost-effective method to modify and enhance the performance of SPEs. Blended polymers typically offer superior physicochemical performance compared to single polymers (Brza et al., 2020). Several studies utilize blended polymers as host polymers, including PEO/PVDF (Patla et al., 2018), PVA/MC (Shamsuri et al., 2020), PVA/chitosan, CMC/chitosan (Hafiza & Isa, 2014), etc. One of the polymers frequently blended with CMC in the SPE development is polyvinyl alcohol (PVA). Several studies utilize blended polymers as host polymers, including PEO/PVDF (Patla et al., 2018), PVA/MC (Shamsuri et al., 2020), PVA/chitosan, CMC/chitosan (Hafiza & Isa, 2014), etc.

Polyvinyl alcohol (PVA) is a polymer synthesized through either partial or complete hydrolysis of polyvinyl acetate (PVAc) (Aruldass et al., 2019). PVA exhibits excellent solubility in water, especially hot water, due to its ability to form hydrogen bonds (O-H) with water molecules (Aruldass et al., 2019), and it has good compatibility with various types of salts due to its ion-dipole interactions with positive ions. Several studies have utilized PVA as a host polymer for solid polymer electrolytes, including PVA/MC (Shamsuri et al., 2020), PVA/PVP (Irfan et al., 2021), PVA/Starch (Gulati et al., 2019), etc. The blending of PVA with CMC (CMC/PVA) is a favoured and extensively studied design due to its non-toxic, easily processable, environmentally degradable properties, and its ability to reduce the crystalline phase of the polymer, thereby achieving good conductivity values (Singh et al., 2022). The blended polymer of CMC/PVA has been investigated as a host polymer for electrolytes in studies such as (Mazuki et al., 2019; Saadiah et al., 2021; Sallal et al., 2022; Gulati et al., 2019).

The selection of proton-sourced salts, such as ammonium salts, is vital for SPE membrane development. Ammonium salts, with low lattice energies, enhance proton conductivity by increasing free ion dissociation (Monisha et al., 2017). Ammonium acetate, with a lattice energy of -500 to -600 kJ/mol, is particularly favorable. These salts release protons through deprotonation, interacting with the host polymer, while the acetate anion also attracts protons via electrostatic interactions (Hemalatha et al., 2019).

This study will investigate the impact of ammonium acetate on an SPE based on a CMC/PVA blend, through molecular vibration studies, ionic conductivity analysis, and physicochemical performance evaluations. The intermolecular interactions between CMC and PVA as host polymers with ammonium acetate are crucial to explore and can be correlated to the resulting physicochemical properties. Characterization methods employed to support this study include functional group analysis, impedance analysis, crystallinity analysis, mechanical analysis, and thermal analysis. This research aims to provide insights into the fundamental behaviour of a proton-conducting SPE membrane based on CMC/PVA/CH_3COONH_4.

EXPERIMENTAL SECTION

Chemicals

The materials used in this work were commercial carboxymethyl cellulose (CMC, Merck), commercial poly(vinyl alcohol) (PVA, Aldrich) with a molecular weight of 145,000 sigma aldrich fully hydrolysed, ammonium acetate 98% (CH_3COONH_4) (Loba Chemie), distilled water, and methanol (CH_3OH) (Merck KGaA) p.a.

Preparation of CMC, CMC/PVA (80/20) and CMC/PVA/CH_3COONH_4-based SPE Membranes

The membranes were prepared by casting solution technique as we many developed in previous work (Darmawan et al., 2024; Ndruru et al., 2022; Ndruru et al., 2023; Ndruru et al., 2024; Ndruru et al., 2023(b); Triandani et al., 2023). Both the CMC membrane and CMC/PVA (80/20) membrane as a control were prepared by dissolving 1 (one) gram of CMC and CMC/PVA mixture with ratio 80/20-wt% were mixed into 40 mL of distilled water at room temperature until homogeneous, respectively. The homogeneous CMC solution was then poured onto the petri dish surface and dried in an oven to remove the solvent at 60 °C for 24 hours.

The CMC/PVA/CH_3COONH_4 SPE membranes were prepared by mixing various weight percentages of CH_3COONH_4 salts (5, 10, 15 and 20 %wt) with CMC/PVA (ratio: 80/20) with a total weight of 1 (one) gram at room temperature until homogeneous. The well mixture was observed by transparent solution which occurred for each composition. The homogeneous CMC/CH_3COONH_4 solution with various compositions was then poured onto the petri dish surface, which was then dried in the oven for at least 24 hours. The dried film was peeled from the petri dish and stored in the free-air room. The result of this stage is a thin film specifically named solid electrolyte membrane.

Characterizations

FTIR spectroscopy

Changes in the surface chemistry of the samples were evaluated using FTIR. Spectra were recorded in the range of 4000-500 cm^{-1} on a Prestige 21 Shimadzu facilitated with an attenuated total reflectance (ATR). From the IR spectra, some physical properties, such as free ion percentage and transport parameters, were calculated according to the following equation, Equation (1) adapted from (Abarna & Hirankumar, 2017):

$$\text{Free ion percentage } (FI\%) = \frac{Free\ ion\ area}{Free\ ion\ area + Contact\ ion\ area} \quad (1)$$

Transmittance intensity can be determined by calculating the peak-to-baseline height on the transmittance scale ($T\%$). The value can be calculated using Equation (2) adapted from (Darmawan et al., 2024)

$$T\% \approx T_{baseline} - T_{peak} \quad (2)$$

The width of the absorption band can be measured by calculating the distance between baselines, which is indicated by Equation (3) adapted from (Hafiza & Isa, 2017)

$$\text{Absorption Bandwidth } (cm^{-1}) = B_f\text{-}B_0 \quad (3)$$

where B_f is the final baseline, and B_0 is the initial baseline.

Transport Parameters

Transport parameters, such as density number (η), mobility (μ), and diffusion coefficient (D) were calculated using Equation (4-6). (31)

$$\text{Ion density } (n) = \left(\frac{mol\ x\ NA}{Vtotal}\right) \text{ x } FI\,(\%) \quad (4)$$

$$\text{Ion mobility } (\mu) = \frac{\sigma}{ne} \quad (5)$$

$$\text{Diffusion coefficient } (D) = \frac{kT\mu}{e} \quad (6)$$

where N_A, V_{total}, e, T, and k represent Avogadro number (mol^{-1}), total volume (mL^{-1}), electric charge (1.62 x 10^{-19}), absolute temperature, Boltzmann constant (1.38 × 10^{-23} JK^{-1}) The force constant (k) is calculated through Hooke's law Equation (7) (Hafiza & Isa, 2017)

$$v = \frac{1}{2\pi c}\sqrt{\frac{k}{\mu}}\ \text{N.cm}^{-1} \quad (7)$$

$$k = 4\pi^2 c^2 v^2 \mu \quad (8)$$

$$\mu = \frac{m_1 \times m_2}{m_1 + m_2} \quad (9)$$

Where, v is the wavenumber (cm^{-1}), c is the speed of light constant (2.998×10^8 $m.s^{-2}$), and μ is the reduced mass.

Ionic Conductivity Analysis

The ionic conductivity of SPE membranes was analysed using an electrochemical impedance spectroscopy (EIS). The AC conductance and impedance data were extracted from LCR-H-tester Hioki 3532-50 at a frequency interval ranging between 42 Hz and 1 MHz. DC ionic conductivity can be determined through its relationship with AC ionic conductivity as follows Equation (10) (Ndruru, Syamsaizar, et al., 2024):

$$\sigma_{AC} = \sigma_{DC} + A\omega^n \quad (10)$$

where: σ_{AC}, σ_{DC}, A, ω, and n refer to AC conductance ($S.cm^{-1}$), DC conductance ($S.cm^{-1}$), angular frequency (rad), and Jonscher power law exponent, respectively. For comparison, DC ionic conductivity can also be determined using a Nyquist plot, according to the Equation (11) (Abdullah et al., 2021) below:

$$\sigma = \frac{t}{R_b x A} \quad (11)$$

where σ, t, R_b, and A represent ionic conductivity ($S.cm^{-1}$), membrane thickness (mm), bulk resistance (ohm), and surface area (cm^2), respectively.

Mechanical Performance

The mechanical properties of SPE membranes were examined using a tensile tester AGS-X. The membranes were prepared with a dimension of 5 × 1 cm and then clamped at a distance of 10 mm with a speed of 10 mm/minute and a cell load of 5 kN. The mechanical strength of the membrane can be calculated by following the Equation (12) (Ndruru et al., 2020).

$$\sigma = \frac{m \times g}{t \times l} \quad (12)$$

where σ, m, g, t, l represents tensile strength (MPa), mass (kg), gravity ($m.s^{-2}$), membrane thickness (mm), and membrane width (in mm), respectively.

Crystallinity Analysis

X-ray Diffraction (XRD). The crystalline structure of SPE membranes was evaluated using XRD PANalytical X'Pert HighScore with Cu Kα source. The diffractogram intensity was recorded as a function of a 2θ interval between 5 and 90°. The crystallinity index (CI, %) of the membranes was quantified according to the following Equation (13) adapted from (Hebbar et al., 2017):

$$C.I.(\%) = \frac{Ac}{Ac + Aa} \times 100\% \quad (13)$$

where A_c and A_a represent the crystalline and amorphous areas.

Thermal Analysis

Thermogravimetry analysis (TGA) and derivative thermal analysis (DTG) were conducted to evaluate the thermal properties of the SPE membranes. The

membrane sample was heated at a temperature in the range of 29-600 °C at a heating rate of 10 C/min under nitrogen (N_2) gas.

RESULT AND DISCUSSION

Surface Chemistry and Molecular Vibrations Study

FTIR Analysis

Figure 1 shows the FTIR spectra for CMC, PVA, CMC/PVA (80/20) blend and CMC/PVA (80/20) + $x$$CH_3COONH_4$ (x = 10, 20, 30 wt/-%). CMC shows some main important functional groups including O-H stretching, C-H stretching of the alkyl group, C=O (carboxylic acid), -CH_2 bending, O-H bending, C-O (ether/carboxylic acid), and C-H bending which are observed at 3441, 2921, 1621, 1420, 1328, 1058, 603 cm^{-1}, respectively(Biswal & Singh, 2004). Poly(vinyl alcohol) exhibits the key vibration absorption including O-H stretching, C-H stretching from alkyl groups, C-O stretching, and C=O stretching which are located at 3425, 2920, 1095, and 849 cm^{-1}, respectively(Awada & Daneault, 2015). CMC/PVA (80/20) blend membrane, meanwhile, displays some deformation on their main peak wavenumber regarding CMC.

The CMC/PVA (80/20) blend membrane shows a split C=O peak due to molecular interactions. A higher wavenumber indicates a free C=O bond, while a lower one shows interaction (Sohaimy et al., 2022). The weakening transmittance intensity at lower wavenumbers suggests decreasing C=O bond strength, especially as CH_3COONH_4 content increases. The lowest force constant, observed at 30wt-% CH_3COONH_4, confirms the interaction, indicating dissociation into NH_4^+ and CH_3COO^- ions. Previous studies confirm that ammonium salt interactions with the host polymer shift the wavenumber lower due to hydrogen bonding with oxygen-containing functional groups (Mazuki et al., 2019; Shukur et al., 2018).

Proton Conductivity Analysis

AC conductance analysis

Figure 2 displays the AC conductance plots which supply the relationship between AC conductance with log angular frequency. The determination of DC proton conductivity was carried out adapting Equation (**10**). DC proton conductivity can be detected by extrapolation method regarding each plot, where the value is located at the plateau segment (Ndruru, et al., 2024). Based on the results, as shown in SI-3, it appears that the incorporation of CH_3COONH_4 impacts the DC proton conductivity change. The highest DC proton conductivity was experienced by 10wt-% of CH_3COONH_4 as high as 3.93×10^{-4} S cm^{-1} and then decreased when the 20wt-% and 30wt-% of CH_3COONH_4. The highest value can be attributed by highest free ion percentage at the compositions that means the composition contributed to ammonium salt dissociation. For comparing to previous research that found that the SPE of CMC/CS showed conductivity of 2.12×10^{-5} S cm^{-1} (Hafiza M.N.1 and Isa M.I.N, 2014), CMC/PVA membrane exhibited the conductivity around 10^{-6} (Saadiah & Samsudin, 2018) and SPE of CMC/PVA doped with NH_4Cl displayed the conductivity of 8.86×10^{-5} S cm^{-1} (Mazuki et al., 2019). Those conductivities were lower than the highest proton conductivity in this study.

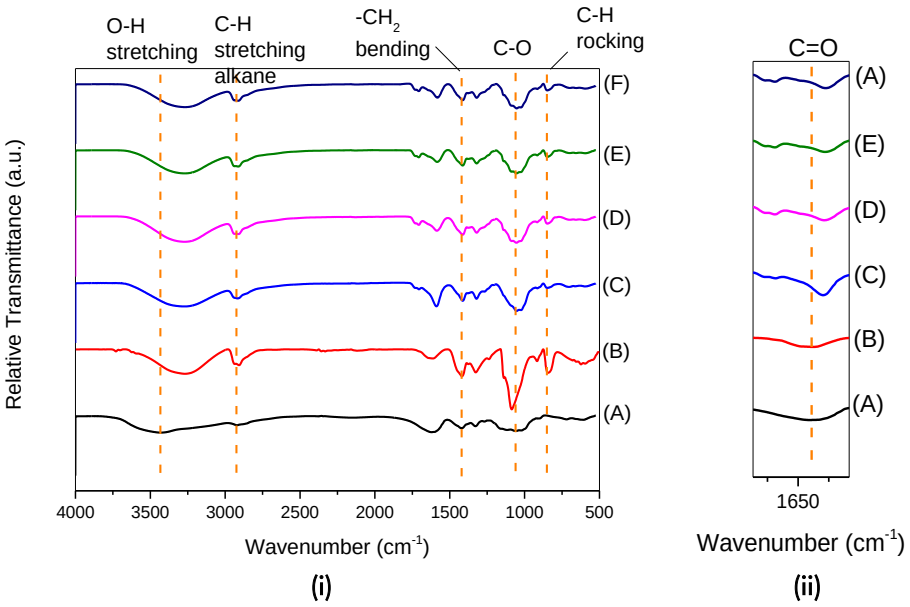

Figure 1 (i) Full spectra and (ii) C=O band spectra for (a) CMC, (b) PVA; (c) CMC/PVA (80:20), (d) CMC/PVA/CH_3COONH_4/(80:20:10), (e) CMC/PVA/CH_3COONH_4 80:20:20), (f) CMC/PVA/CH_3COONH_4 (80:20:30).

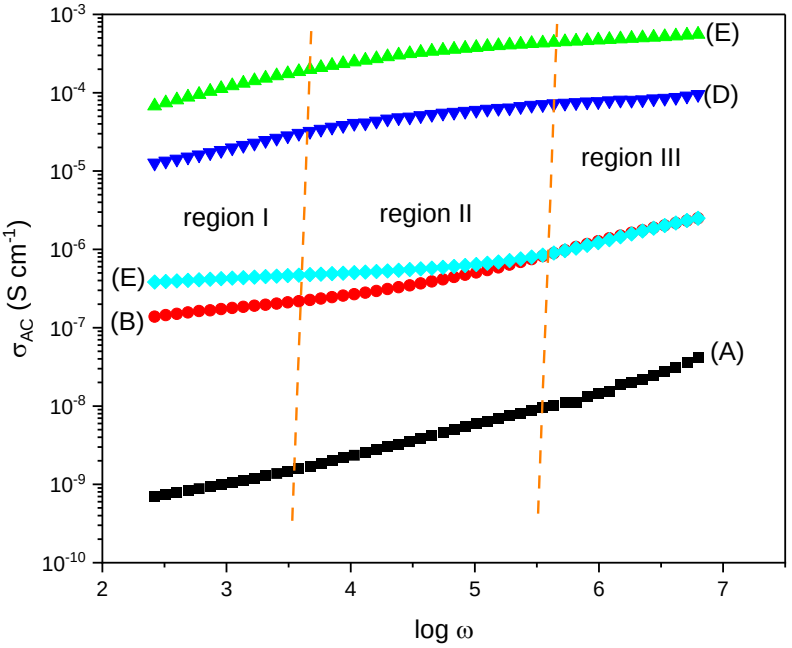

Figure 2 AC conductance plot for (A) CMC 100%; (B) CMC/PVA (80/20) blend and complexed with CH_3COONH_4 for each (C) 10wt-%; (D) 20wt-% and (E) 30wt-%

The excess of CH_3COONH_4 incorporation caused the DC proton conductivity to decrease gradually decreased. The abundance of ammonium salt can't be dissociated by the system. This condition has ever been reported in previous work, where the addition of 50wt-% NH_4SCN into PAN/PVP (80/20) blend SPE membrane, after optimum condition, caused resistance increase. The excess of NH_4SCN in this composition makes ions agglomeration, which reduces the ion mobilisation (Daniel et al., 2023). As commonly known, the ion or proton conductivity was influenced by some important factors, including ionic species conducting ions concentration, the charge carriers types (either cationic or anionic), the mobility of charge carriers, and the temperature (Rasali et al., 2020).

Figure 2 also exhibits the different regions observed. Region I at the low frequency explains the internal phenomena between electrode-SPE membranes. In this space, the space charge polarization/electrode polarization occurred, where protons have sufficient time to accumulate in the electrode/SPE membrane interface, and no available ions are mobile. Region II is the plateau space, where the DC conductivity is obtained. Meanwhile, Region III at the highest frequency is the dispersion region, where further increased conductivity appeared (Shetty et al., 2021). Region I and II are expressed by the jump relaxation model, where protons jump from one coordinate site to another vacant neighbouring in the SPE matrix (Shetty et al., 2021). In this work, SPE membranes have some polar groups which are supplied by CMC and PVA polymer chain as polymer chain, as explained previous section. As commonly known, solid polymer electrolytes (SPEs) should meet several criteria. Besides having a low glass transition temperature, the polymer should provide low cohesive energy to facilitate salt dissociation. Additionally, it should possess a large number of polar groups, such as O-H, -C=O, and O=C-OH groups, along with a flexible polymer chain.

Nyquist plot analysis

Figure 3 exhibits the Nyquist plot for all membranes, including CMC, CMC/PVA (80/20) blend membrane and CMC/PVA (80/20) blend + various weight percentages of CH_3COONH_4 SPE membrane. CMC shows the highest resistance which exhibits the lowest proton conductivity as high as 1.16×10^{-9} S cm^{-1}. The resistance decrement happened when it blends to PVA with the ratio 80/20. The CMC/PVA (80/20) blend offered lower resistance which was indicated by increasing the DC conductivity as much as 3.20×10^{-6}. The DC conductivity for both the CMC membrane and CMC/PVA (80/20) is appropriate as a total conductivity, because the ammonium acetate, as a dopant, still does not exist inside.

The Nyquist plot shows improved DC conductivity after incorporating CH_3COONH_4 into the host polymer. The 10wt-% CH_3COONH_4-complexed CMC/PVA blend exhibits the highest DC proton conductivity at 7.96×10^{-4} S cm^{-1}. This increase is due to enhanced amorphous regions and chain flexibility. However, conductivity decreases at higher CH_3COONH_4 concentrations, with 20wt-% showing 1.08×10^{-5} S·cm^{-1} and 30wt-% dropping to 5.45×10^{-6} S·cm^{-1}. The change in conductivity is attributed to the percentage of free ions, with 10wt-% CH_3COONH_4 yielding the highest free ion percentage.

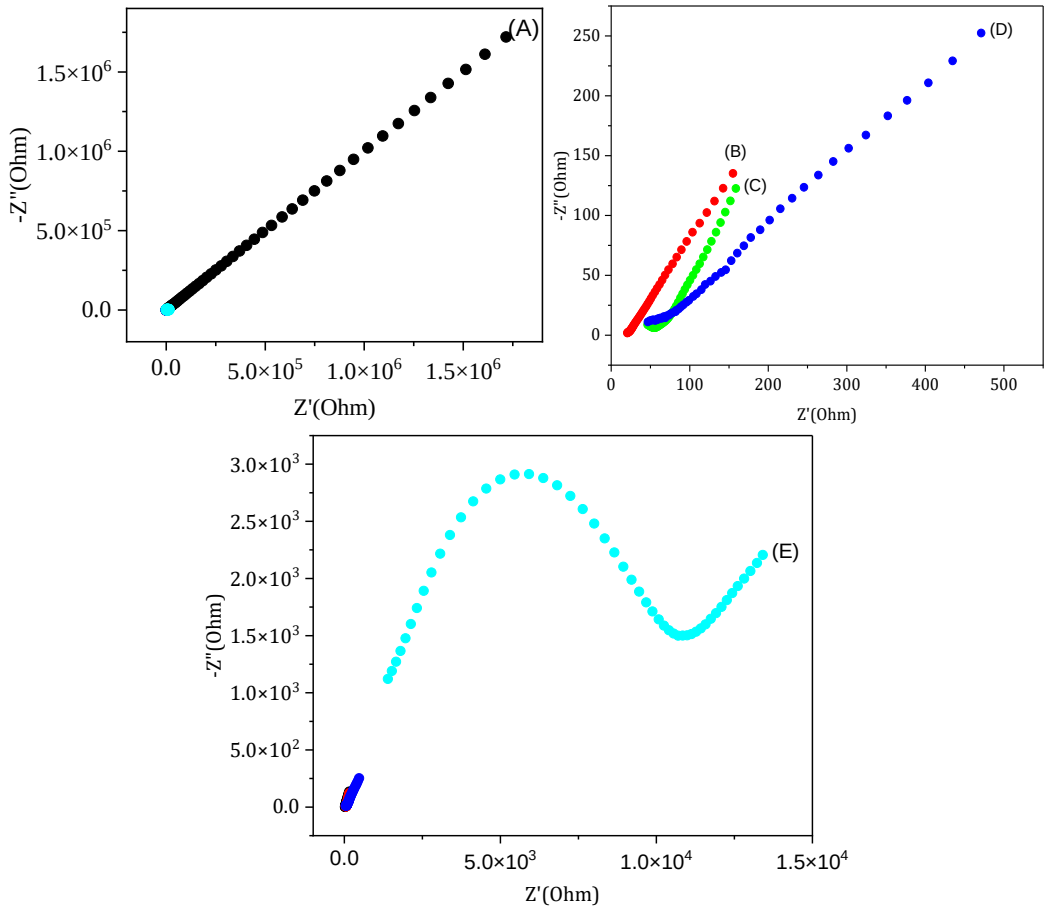

Figure 3 Nyquist plot for (A) CMC membrane, (B) CMC/PVA (80/20) membrane, (C) CMC/PVA (80/20) + 10wt-% CH_3COONH_4; (D) CMC/PVA (80/20) + 20wt-% CH_3COONH_4 and (E) CMC/PVA (80/20) + 30wt-% CH_3COONH_4

The Nyquist plot, commonly, explains the diverse phenomena. A semicircle at the high-frequency region due to the bulk effect of the CPEs, and a tail were observed in the low-frequency region. Additionally, there was an incomplete semicircle at higher frequencies, primarily related to the bulk properties (bulk resistance) of the materials. At low frequencies, a spike was noted, indicating double-layer capacitance at the electrode/sample interface (Cyriac et al., 2022). The spike (tail) in the low-frequency region results from the accumulation of free charges at the electrode and electrolyte interface, leading to the formation of an EDLC (Ahmed et al., 2022). When an AC electric field is applied to the membrane electrolytes, ion diffusion occurs across the membrane, leading to ion accumulation at the electrode/electrolyte interface. Due to the electronic nature of the stainless-steel electrodes, ions cannot pass through them. This allows for the measurement of the real and imaginary components of impedance at various frequencies, resulting in impedance graphs. By intersecting the spike with the plot's real axis, the R_b values were determined from the data analysis (Ahmed et al., 2022).

This spike is visible in all other samples. In this work, a disappeared semicircle curve was seen at the 10wt-% and 20wt-% CH_3COONH_4 incorporation, which indicated the SPE membrane resistance decrease. The semicircle was observed when the highest CH_3COONH_4 incorporation, which confirm internal resistance back increased, as saturation condition of ion-pair formation.

Figure 4 serves the possible interaction mechanism of CMC, PVA and CH_3COONH_4 including the proton hopping mechanism and mobilization. Ammonium cations experience de-protonation to supply proton in the SPE system, so the proton is hopping from CMC and PVA polar groups such as –OH, -O-, C=O and $–COO^-$. The ionic hopping mechanism in polymer electrolytes is driven by the movement of mobile charge carriers or ions that dissociate from complexes. For ionic conduction through hopping to occur, certain fundamental conditions must be met: there must be mobile ions available for migration and vacant sites for these ions to occupy (Dennis et al., 2023).

Physical Properties of SPE Membranes

Mechanical performance

Mechanical properties analysis is one of the crucial aspects of the quality of SPE membranes. The representative of mechanical performance for all

membrane samples was presented in Figure 5 and extracted into **Table 1**. Pure CMC membrane shows a high tensile strength, moderate elongation and Young's modulus. As a standard, it shows more flexible than its blend with PVA (CMC/PVA). The existence of a CMC/PVA (80/20) blend membrane exhibited a change in mechanical properties. The tensile strength decrement in the CMC/PVA (80/20) was not followed by the elongation at break increment, on the other side Young's modulus increased. The high Young's modulus indicates the rigidity performance increment as crystallinity index (C.I.) consequence which will discussed in previous section.

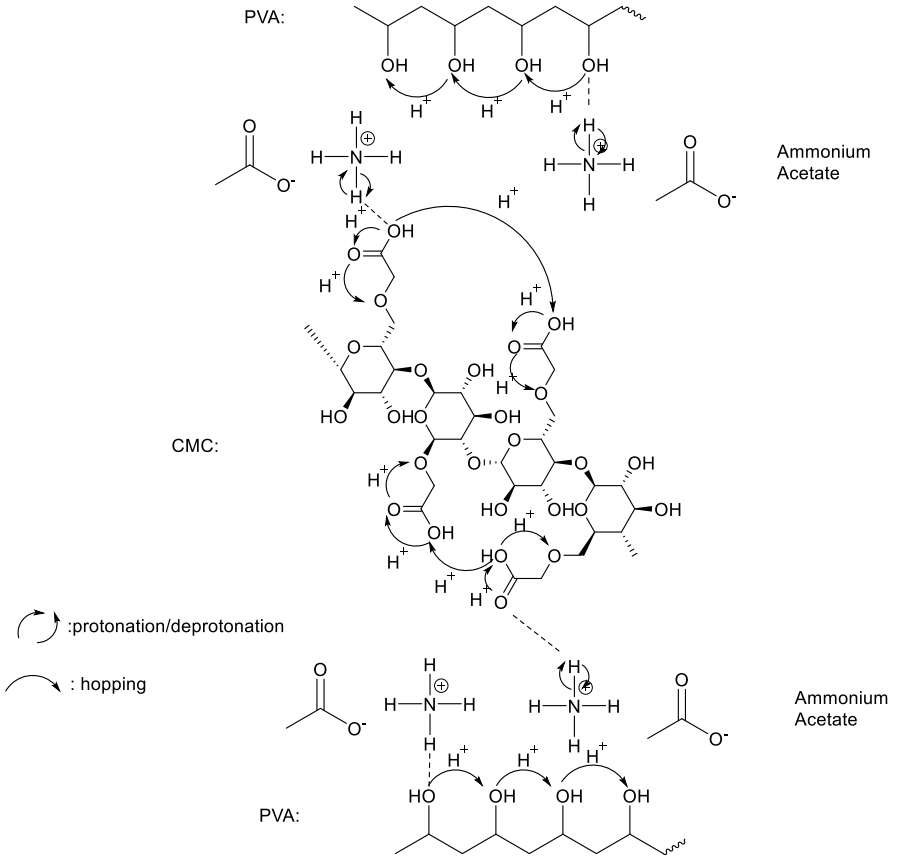

Figure 4 Possible interaction mechanisms of CMC, PVA and CH_3COONH_4

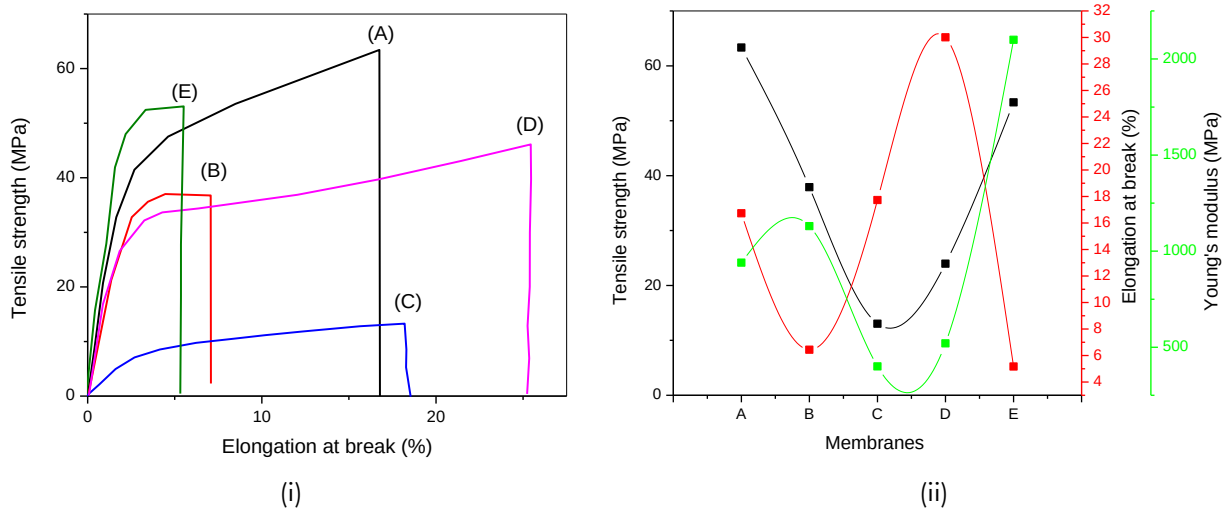

Figure 5. (i) Representative Plot of Tensile Strength vs Elongation at break and (ii) The relationship Tensile strength regards Elongation at break and Young's modulus for (A) Pure CMC membrane, (B) CMC/PVA (80/20) blend membrane, (C) SPE of CMC/PVA/CH_3COONH_4 (80/20/10), (D) SPE of CMC/PVA/CH_3COONH_4 (80/20/20), (E) SPE of CMC/PVA/CH_3COONH_4 (80/20/30)

Table 1. Mechanical analysis of SPE membrane of CMC/PVA/ CH_3COONH_4

Membrane	Tensile Strength (MPa)	Elongation at Break (%)	Young's Modulus (MPa)
Pure CMC membrane	63.33	16.73	940
CMC/PVA (80/20)	37.90	6.44	1130
CMC/PVA (80/20) + 10 %wt CH_3COONH_4	13.03	17.73	400
CMC/PVA (80/20) + 20 %wt CH_3COONH_4	23.98	30.01	520
CMC/PVA (80/20) + 30 %wt CH_3COONH_4	53.34	5.17	2100

The incorporation of CH_3COONH_4 into the CMC/PVA (80/20) host polymer significantly impacts the mechanical properties of the SPE membrane. The highest flexibility, with the lowest tensile strength and moderate elongation, occurred at 10wt-% CH_3COONH_4. At this composition, the salt disrupts hydrogen bonding between CMC and PVA, promoting an amorphous region, which inhibits crystallization, as will be discussed further (Cyriac et al., 2022).

At 20wt-% CH_3COONH_4, the interaction between the salt and host polymer decreased, while hydrogen bonding strengthened, leading to ion-pair formation. Maximum rigidity was observed at 30wt-%, where excess CH_3COONH_4 caused ion agglomeration, hindering segmental motion and ionic conduction. This increased tensile strength and Young's modulus but reduced elongation at break (Daniel et al., 2023)(Tan et al., 2020)(Shyly et al., 2022). The mechanical properties change is correlated with the crystallinity properties.

As explained earlier, high salt concentrations lead to ion association, reducing the number of charge carriers and decreasing conductivity (σ) while increasing R_b. The rise in polymer electrolyte crystallinity at high salt levels further limits ion mobility, as the amorphous phase facilitates ion movement, contributing to the higher R_b value (M. A. Brza et al., 2020).

Crystalline properties analysis

X-ray diffraction (XRD) analysis was performed to understand the crystallinity patterns and properties of the pure CMC as host polymer, CMC/PVA (80/20) blend membrane, and the CH_3COONH_4 (10, 20, 30 wt%)-complexed CMC/PVA (80/20) blend membrane as presented in Figure 6. The deconvolution method in this work was used to determine the crystallinity index for all compositions (Borodin & Smith, 2006). XRD pattern of CMC shows a crystalline peak at $2\theta = 21.6°$ (de Oliveira Barud et al., 2016), while the CMC/PVA (80/20) blend shows a crystalline peak at 22.64°. The addition of CH_3COONH_4 salt affects to crystalline peak shift at 2θ: 10-30°. The addition of 10wt-% CH_3COONH_4 salt showed a crystalline peak at 20.61°. The addition of 20wt-% CH_3COONH_4 salt has a crystalline peak at 20.51°. The addition of 30wt-% CH_3COONH_4 salt showed a crystalline peak at 20.36°. The addition of CH_3COONH_4 salt to the CMC PVA blend experienced a peak shift indicating an interaction between the salt and the polymer (Kumar et al., 2017).

Deconvoluted XRD spectra were conducted to determine the crystallinity index (*C.I.*). The crystallinity index determination of the host polymer CMC, CMC/PVA blend (80/20) and CMC/PVA blend complexed with various weight percentages of CH_3COONH_4 were determined using Equation (**13**). Based on the calculation, CMC showed the highest crystallinity index as high as 60.30%, while its blend to the PVA exhibited a lower crystallinity index as high as 30.11%. The further incorporation of CH_3COONH_4 caused a lower crystallinity index to continue as high as 12.94%. The crystallinity index decreasing, generally, causes the flexibility to increase and improves the conductivity (Rasali et al., 2020). The lower crystallinity index also indicates that salt was completely dissolved in the system, as explained in previous work, where NaI had perfectly dissolved in the PVA-based SPEs and contributed to amorphous region formation (Ahmed et al., 2022). The flexibility of the amorphous polymer chain segment contributes to enlarged free volume (Ramlli & Isa, 2016).

Meanwhile, the further incorporation of 20wt-% and 30wt-% rearranges the polymer chain interaction, causing the crystallinity index to increase as high as 29.79% and 41.89%, respectively. The increase of crystallinity index of the present sample provides lesser free volume which in turn decreases the ionic conductivity upon the addition of ammonium salt at a lower composition (Mazuki et al., 2019). Previous work revealed that the 30 and 40 wt.% of NH_4BF_4 caused more crystalline and high-intensity peaks as indicated in the XRD spectra (Brza et al., 2020).

Thermogravimetry Analysis (TGA)

Besides good mechanical performance at high temperatures, the polymer electrolyte must have high thermal stability to prevent thermal runaway reactions in lithium-ion batteries (Xiong et al., 2014). Thermal degradation, generally, consists of some stages, including dehydration, depolymerization, the

glycosidic units decomposition and the formation of carbon residue (Shaikh et al., 2022). On the other hand, the decomposition temperature indicates that the polymer membranes break down into oligomers and monomers, leading to thermal runaway (Yazie et al., 2023). Thermogravimetric analysis (TGA) is a technique in which a material is subjected to controlled heating, causing its decomposition and the subsequent breaking of molecular bonds. This method is fundamental for assessing the thermal stability of materials. TGA curves and DTG (first TGA derivatives) of SPE membranes are presented in **Figure 7** and tabulated in **Table 2**. As the host polymer, CMC experiences water removal below 200°C as high as 10-15%. The first degradation phase at 266.21 - 312.05 °C is the decomposition of the CMC-polymer chain with the maximum degradation rate occurring at 273.18. The decarboxylation thermal decomposition occurs at 479.65 °C.

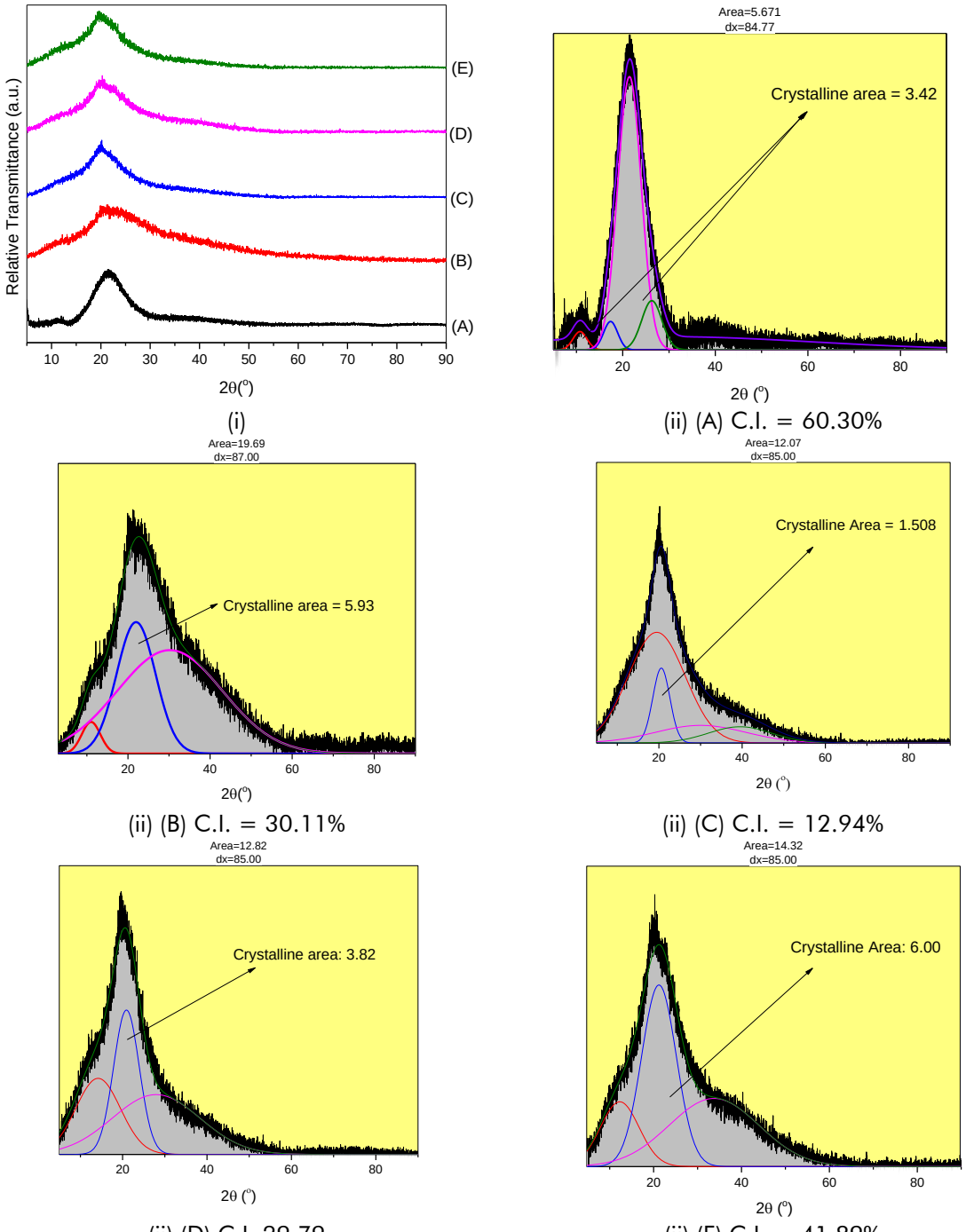

Figure 6. (i) XRD spectra and (ii) Deconvoluted-XRD spectra for (A) pure CMC; (B) CMC/PVA (80/20); (C) CMC/PVA (80/20) + 10% wt CH_3COONH_4; (D) CMC/PVA (80/20) + 20 %wt CH_3COONH_4 and (E) CMC/PVA (80/20) + 30 %wt CH_3COONH_4

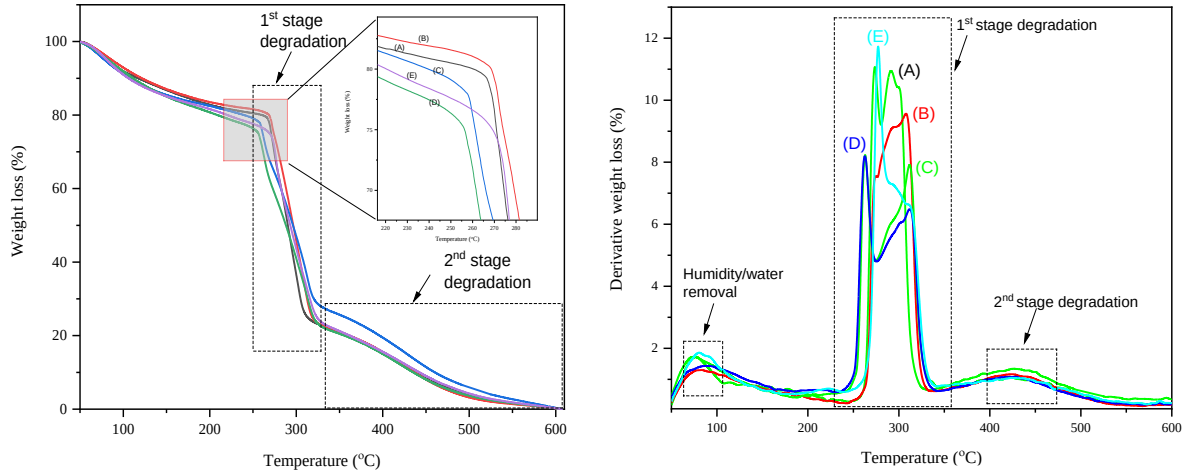

Figure 7. Thermogram of (a) TGA and (b) DTG for (A) pure CMC; (B) CMC/PVA (80/20); (C) CMC/PVA (80/20) + 10% wt CH_3COONH_4; (D) CMC/PVA (80/20) + 20 %wt CH_3COONH_4 and (E) CMC/PVA (80/20) + 30 %wt CH_3COONH_4

Table 2. Decomposition temperature for CMC, CMC/PVA blend and CH_3COONH_4-complexed CMC/PVA (80/20) blend

Membrane composition	T_{onset} (°C)	T_{offset} (°C)	$T_{max\ 1}$ (°C)	$T_{max\ 2}$ (°C)
CMC (100)	266.21	312.05	273.18	292.04
CMC/PVA (80/20)	268.12	319.68	307.67	-
CMC/PVA (80/20) + 10wt%-CH_3COONH_4	258.04	320.82	263.15	311.98
CMC/PVA (80/20) + 20wt%-CH_3COONH_4	255.56	321.89	262.46	311.75
CMC/PVA (80/20) + 30wt%-CH_3COONH_4	269.91	324.75	276.84	-

The CMC/PVA (80:20) blend membrane degrades from 268.12 to 319.68 °C with weight loss of as much as 55.45%. The maximum degradation rate can appear at 307.67%, indicating the main polymer-chain degradation. The onset degradation temperature of the CMC/PVA (80/20) blend membrane has a higher temperature compared to pure CMC-based membrane. The combination of PVA into the blend membrane contributes to an increase in the onset degradation temperature. Previous work revealed that the polymer blending technique is an important technique to improve the thermal stability of polymer electrolytes (Yazie et al., 2023). The thermal stability of polymer blends is influenced by the bond energies within their high molecular weight structures, the types of intra- and intermolecular forces, the degree of unsaturation and branching, the length of polymerization segments, their composition, and the degree of crystallization in the blends (Yazie et al., 2023; Stivala & Reich, 1980; Tomić, 2019).

The SPE membrane of 10wt-% CH_3COONH_4-complexed CMC/PVA (80/20) blend started to degrade first at 258.04 to 320.82 °C with weight loss of as much as 49%, and the maximum degradation rate can be observed at 263.15 °C. The addition of 20wt-% CH_3COONH_4-complexed CMC/PVA (80/20) blend started to degrade at 255.56 to 321.89 °C with weight loss as high as 51.84% and the maximum degradation rate can be observed at 262.46 and 311.75°C. The addition of 10wt-% and 20wt-% salt decreased the thermal stability. This is due to the formation of complexation between the ammonium cation (NH_4^+) of ammonium acetate salt with the hydroxyl group of the polymer (Hirankumar et al., 2005).

The addition of 30wt-% CH_3COONH_4 salt started to degrade at 269.91 to 324.75 °C with weight loss as high as 50.19%, and the maximum degradation rate can be observed at 276.84°C. In line with some characterization results, the addition of 30wt-% CH_3COONH_4 incorporation has high stability which previously correlated with the molecular interaction and physical performance such as tensile strength and crystalline performance. The thermal stability could be attributed to strong hydrogen bond interaction, rigidity and high crystallinity index. Previous work found that the incorporation of filler enhanced the thermal stability of polymer electrolytes (Shyly et al., 2022).

CONCLUSIONS

The SPE membranes' molecular vibrations and physicochemical performance were evaluated. SPE

membranes of CMC/PVA (80/20) blend complexed to various weight percentages (10, 20, and 30wt-%) of CH_3COONH_4 salt were prepared by using the casting solution method. Based on the results, the 10wt-% CH_3COONH_4-complexed CMC/PVA (80/20) has the highest proton conductivity of 3.93×10^{-4} S/cm with tensile strength of 13.03 MPa and lower Young's modulus of 400 MPa among others. Its higher ionic conductivity was influenced by the crystallinity index decrement of 12.94%, but it still offers good thermal stability at intervals 258.04 – 320.82 °C. Further characterization should be conducted to support its application for proton batteries.

ACKNOWLEDGEMENTS

Authors acknowledge Lembaga Pengelola Dana Pendidikan, Ministry of Finance Affairs through the Riset dan Inovasi untuk Indonesia Maju (RIIM) 2 join to National Research and Innovation Agency (BRIN) for providing research funding.

REFERENCES

Abarna, S., & Hirankumar, G. (2017). Vibrational, electrical, and ion transport properties of PVA-LiClO4-sulfolane electrolyte with high cationic conductivity. *Ionics*, *23*(7), 1733–1743. https://doi.org/10.1007/s11581-017-2008-y

Abdullah, A. M., Aziz, S. B., & Saeed, S. R. (2021). Structural and electrical properties of polyvinyl alcohol (PVA):Methyl cellulose (MC) based solid polymer blend electrolytes inserted with sodium iodide (NaI) salt. *Arabian Journal of Chemistry*, *14*(11), 103388. https://doi.org/10.1016/j.arabjc.2021.103388

Ahmed, M. B., Nofal, M. M., Aziz, S. B., Al-Saeedi, S. I., Brza, M. A., Dannoun, E. M. A., & Murad, A. R. (2022). The study of ion transport parameters associated with dissociated cation using EIS model in solid polymer electrolytes (SPEs) based on PVA host polymer: XRD, FTIR, and dielectric properties. *Arabian Journal of Chemistry*, *15*(11), 104196. https://doi.org/10.1016/j.arabjc.2022.104196

Akhlaq, M., Mushtaq, U., Naz, S., & Uroos, M. (2023). Carboxymethyl Cellulose-based Materials as an Alternative Source for Sustainable Electrochemical Devices: A Review. *RSC Advances*, *13*, 5723–5743.

Aruldass, S., Mathivanan, V., Mohamed, A. R., & Tye, C. T. (2019). Factors affecting hydrolysis of polyvinyl acetate to polyvinyl alcohol. *Journal of Environmental Chemical Engineering*, *7*(5), 103238. https://doi.org/10.1016/j.jece.2019.103238

Awada, H., & Daneault, C. (2015). Chemical modification of poly(vinyl alcohol) in water. *Applied Sciences (Switzerland)*, *5*(4), 840–850. https://doi.org/10.3390/app5040840

Biswal, D. R., & Singh, R. P. (2004). Characterisation of carboxymethyl cellulose and polyacrylamide graft copolymer. *Carbohydrate Polymers*, *57*(4), 379–387. https://doi.org/10.1016/j.carbpol.2004.04.020

Borodin, O., & Smith, G. D. (2006). Mechanism of Ion Transport in Amorphous Poly(ethylene oxide)/LiTFSI from Molecular Dynamics Simulations. *Macromolecules*, *39*(4), 1620–1629. https://doi.org/10.1021/ma052277v

Brza, M. A., Aziz, S. B., Nofal, M. M., Saeed, S. R., Al-Zangana, S., Karim, W. O., Hussen, S. A., Abdulwahid, R. T., & Kadir, M. F. Z. (2020). Drawbacks of low lattice energy ammonium salts for ion-conducting polymer electrolyte preparation: Structural, morphological and electrical characteristics of CS:PEO:NH4BF4-based polymer blend electrolytes. *Polymers*, *12*(9), 1-21. https://doi.org/10.3390/POLYM1209 1885

Brza, M., Aziz, S. B., Saeed, S. R., Hamsan, M. H., Majid, S. R., Abdulwahid, R. T., Kadir, M. F. Z., & Abdullah, R. M. (2020). Energy storage behavior of lithium-ion conducting poly(Vinyl alcohol) (pva): Chitosan(cs)-based polymer blend electrolyte membranes: Preparation, equivalent circuit modeling, ion transport parameters, and dielectric properties. *Membranes*, *10*(12), 1–20. https://doi.org/10.3390/membranes10120381

Cyriac, V., Ismayil, Noor, I. M., Mishra, K., Chavan, C., Bhajantri, R. F., & Masti, S. P. (2022). Ionic conductivity enhancement of PVA: carboxymethyl cellulose poly-blend electrolyte films through the doping of NaI salt. *Cellulose*, *29*(6), 3271–3291. https://doi.org/10.1007/s10570-022-04483-z

Daniel, R., Priscilla, S. J., Karthikeyan, S., Selvasekarapandian, S., Sivaji, K., & Madeswaran, S. (2023). Synthesis of Solid Polymer Blend Electrolytes Based on PVP/PAN/Ammonium Thiocyanate: Structural, Electrical, Dielectric and Electrochemical Analysis. *Asian Journal of Chemistry*, *35*(1), 159–164. https://doi.org/10.14233/ajchem.2023.24022

Darmawan, D. A., Yulianti, E., Sabrina, Q., Ishida, K., Sakti, A. W., Nakai, H., Pramono, E., & Ndruru, S. T. C. L. (2024). Fabrication of solid polymer electrolyte based on carboxymethyl cellulose complexed with lithium acetate salt as Lithium-ion battery separator. *Polymer Composites*, *45*(3), 2032–2049. https://doi.org/10.1002/pc.27902

de Oliveira Barud, H. G., da Silva, R. R., da Silva Barud, H., Tercjak, A., Gutierrez, J., Lustri, W. R., de Oliveira, O. B., & Ribeiro, S. J. L. (2016). A multipurpose natural and renewable polymer in medical applications: Bacterial

cellulose. *Carbohydrate Polymers*, *153*, 406–420. https://doi.org/10.1016/j.carbpol.2016.07.059

Dennis, J. O., Shukur, M. F., Aldaghri, O. A., Ibnaouf, K. H., Adam, A. A., Usman, F., Hassan, Y. M., Alsadig, A., Danbature, W. L., & Abdulkadir, B. A. (2023). A Review of Current Trends on Polyvinyl Alcohol (PVA)-Based Solid Polymer Electrolytes. *Molecules*, *28*(4), 1-47, https://doi.org/10.3390/molecules28041781

Di Noto, V., Lavina, S., Giffin, G. A., Negro, E., & Scrosati, B. (2011). Polymer electrolytes: Present, past and future. *Electrochimica Acta*, *57*(1), 4–13. https://doi.org/10.1016/j.electacta.2011.08.048

Fu, X., Li, Y., Liao, C., Gong, W., Yang, M., Li, R. K. Y., Tjong, S. C., & Lu, Z. (2019). Enhanced electrochemical performance of solid PEO/$LiClO_4$ electrolytes with a 3D porous Li6.28La3Zr2Al0.24O12 network. *Composites Science and Technology*, *184*. https://doi.org/10.1016/j.compscitech.2019.107863

Gulati, K., Lal, S., & Arora, S. (2019). Synthesis and characterization of PVA/Starch/CMC composite films reinforced with walnut (Juglans regia L.) shell flour. *SN Applied Sciences*, *1*(11). https://doi.org/10.1007/s42452-019-1462-8

Hafiza, M. N., & Isa, M. I. N. (2017). Solid polymer electrolyte production from 2-hydroxyethyl cellulose: Effect of ammonium nitrate composition on its structural properties. *Carbohydrate Polymers*, *165*, 123–131. https://doi.org/10.1016/j.carbpol.2017.02.033

Hafiza, M.N.1 & Isa, M.I.N. (2014). Ionic Conductivity and Conduction Mechanism Studies of CMC/ Chitosan Biopolymer Blend Electrolytes. *Research Journal of Recent Sciences Res.J.Recent Sci*, *3*(11), 50–56.

Hebbar, V., Bhajantri, R. F., & Naik, J. (2017). Physico-chemical properties of Bismuth nitrate filled PVA–LiClO4 polymer composites for energy storage applications. *Journal of Materials Science: Materials in Electronics*, *28*(8), 5827–5839. https://doi.org/10.1007/s10854-016-6254-y

Hemalatha, R., Alagar, M., Selvasekarapandian, S., Sundaresan, B., & Moniha, V. (2019). Studies of proton conducting polymer electrolyte based on PVA, amino acid proline and NH 4 SCN. *Journal of Science: Advanced Materials and Devices*, *4*(1), 101–110. https://doi.org/10.1016/j.jsamd.2019.01.004

Hirankumar, G., Selvasekarapandian, S., Kuwata, N., Kawamura, J., & Hattori, T. (2005). Thermal, electrical and optical studies on the poly(vinyl alcohol) based polymer electrolytes. *Journal of Power Sources*, *144*(1), 262–267. https://doi.org/10.1016/j.jpowsour.2004.12.019

Hoang Huy, V. P., So, S., & Hur, J. (2021a). Inorganic Fillers in Composite Gel Polymer Electrolytes for High-Performance Lithium and Non-Lithium Polymer Batteries. *Nanomaterials*, *11*(3), 614. https://doi.org/10.3390/nano11030614

Hoang Huy, V. P., So, S., & Hur, J. (2021b). Inorganic Fillers in Composite Gel Polymer Electrolytes for High-Performance Lithium and Non-Lithium Polymer Batteries. *Nanomaterials*, *11*(3), 614. https://doi.org/10.3390/nano11030614

Irfan, M., Manjunath, A., Mahesh, S. S., Somashekar, R., & Demappa, T. (2021). Influence of NaF salt doping on electrical and optical properties of PVA/PVP polymer blend electrolyte films for battery application. *Journal of Materials Science: Materials in Electronics*, *32*(5), 5520–5537. https://doi.org/10.1007/s10854-021-05274-1

Kumar, R., Sharma, S., Pathak, D., Dhiman, N., & Arora, N. (2017). Ionic conductivity, FTIR and thermal studies of nano-composite plasticized proton conducting polymer electrolytes. *Solid State Ionics*, *305*(January), 57–62. https://doi.org/10.1016/j.ssi.2017.04.020

Li, J., Yan, H., Xu, C., Liu, Y., Zhang, X., Xia, M., Zhang, L., & Shu, J. (2021). Insights into host materials for aqueous proton batteries: structure, mechanism and prospect. *Nano Energy*, *89*, 106400. https://doi.org/10.1016/j.nanoen.2021.106400

Lizundia, E., & Kundu, D. (2021). Advances in Natural Biopolymer-Based Electrolytes and Separators for Battery Applications. *Advanced Functional Materials*, *31*(3), 1–29. https://doi.org/10.1002/adfm.202005646

Mazuki, N. F., Fuzlin, A. F., Saadiah, M. A., & Samsudin, A. S. (2019). An investigation on the abnormal trend of the conductivity properties of CMC/PVA-doped NH4Cl-based solid biopolymer electrolyte system. *Ionics*, *25*(6), 2657–2667. https://doi.org/10.1007/s11581-018-2734-9

Monisha, S., Mathavan, T., Selvasekarapandian, S., Milton Franklin Benial, A., Aristatil, G., Mani, N., Premalatha, M., & Vinoth pandi, D. (2017). Investigation of bio polymer electrolyte based on cellulose acetate-ammonium nitrate for potential use in electrochemical devices. *Carbohydrate Polymers*, *157*(3), 38–47. https://doi.org/10.1016/j.carbpol.2016.09.026

Nagao, Y. (2024). Proton-Conducting Polymers: Key to Next-Generation Fuel Cells, Electrolyzers, Batteries, Actuators, and Sensors. *ChemElectroChem*, *11*(12). https://doi.org/10.1002/celc.202300846

Ndruru, S. T. C. L., Asta, V. A., Hidayat, Rifa Al Razi Mawarni, Rista Siti Marlina, Anita Yulianti, Evi Handayani, Aniek Sri Hikmat Siregar, Rabiyatul Adawiyah Heliawati, Leny Kareem, A. A., Wihadi, M. N. K., Hayati, A. T., & Prasetyo, R. (2024). Isolation , Modification , and Characterization of Local Indonesia ' s Sugarcane Bagasse Cellulose for Dye-Adsorbent Application. *ChemistrySelect*, *202302812*(9), 1–13. https://doi.org/10.1002/slct.202302812

Ndruru, S. T. C. L., Bundjali, B., & Wahyuningrum, D. (2022). The effect of [EMIm]BF4/ Li+ Ionic liquid on PEO-based solid polymer electrolyte membranes characteristics as lithium-ion batteries separator. *Indian Journal of Engineering and Materials Sciences*, *29*(2), 271–282.

Ndruru, S. T. C. L., Marlina, A., Nugroho, B. S., Pramono, E., Sabrina, Q., Yulianti, E., Arcana, I. M., & Wahyuningrum, D. (2023). Preparation and characterization of polymer blend electrolyte membranes based on lithium acetate-complexed carboxymethyl cellulose (<scp>CMC</scp>) and carboxymethyl chitosan (<scp>CMCh</scp>) blend. *Polymer Engineering & Science*, *64*(2), 761–778. https://doi.org/10.1002/pen.26582

Ndruru, S. T. C. L., Syamsaizar, A. D., Hermanto, S., Sitanggang, B. C., Tawa, B. D., Kareem, A. A., Hayati, A. T., Ramadhoni, B. F., Sofyan, M. I., Annas, D., Prasetyo, J., Marlina, A., Sabrina, Q., Yulianti, E., Sudaryanto, Wahyuningrum, D., & Arcana, I. M. (2024). Synthesis of carboxymethyl cellulose from coconut fibers and its application as solid polymer electrolyte membranes. *Journal of Applied Polymer Science*, *141*(28), 1–22. https://doi.org/10.1002/app.55629

Ndruru, S. T. C. L., Wahyuningrum, D., Bundjali, B., & Arcana, I. M. (2020). Preparation and characterization of biopolymer electrolyte membranes based on liclo4-complexed methyl cellulose as lithium-ion battery separator. *Journal of Engineering and Technological Sciences*, *52*(1), 28–50. https://doi.org/10.5614/j.eng.technol.sci.2020.52.1.3

Ndruru, S. T. C. L., Wahyuningrum, D., Bundjali, B., & Arcana, I. M. (2023). The Utilization of Nias Indonesia's Cacao Pod Husk Cellulose Derivative as Blend Agent for MC/CMC Blend-based Membranes. *The 8th International Symposium on Applied Chemistry (ISAC) 2022*, *2902*, 050001. https://doi.org/10.1063/5.0172838

Ngai, K. S., Ramesh, S., Ramesh, K., & Juan, J. C. (2016). A review of polymer electrolytes: fundamental, approaches and applications. *Ionics*, *22*(8), 1259–1279. https://doi.org/10.1007/s11581-016-1756-4

Nofal, M. M., Karim, W. O., Asnawi, A. S. F. M., Hadi, J. M., Fakhrul, M., & Abdul, Z. (2021). A Polymer Blend Electrolyte Based on CS with Enhanced Ion Transport and Electrochemical Properties for Electrical Double Layer Capacitor Applications. *Polymers*, *13*(6), 930.

Patla, S. K., Ray, R., Asokan, K., & Karmakar, S. (2018). Investigation of ionic conduction in PEO-PVDF based blend polymer electrolytes. *Journal of Applied Physics*, *123*(12). https://doi.org/10.1063/1.5022050

Ramlli, M. A., & Isa, M. I. N. (2016). Structural and ionic transport properties of protonic conducting solid biopolymer electrolytes based on carboxymethyl cellulose doped with ammonium fluoride. *Journal of Physical Chemistry B*, *120*(44), 11567–11573. https://doi.org/10.1021/acs.jpcb.6b06068

Rasali, N. M. J., Saadiah, M. A., Zainuddin, N. K., Nagao, Y., & Samsudin, A. S. (2020). Ionic transport studies of solid bio-polymer electrolytes based on carboxymethyl cellulose doped with ammonium acetate and its potential application as an electrical double layer capacitor. *Express Polymer Letters*, *14*(7), 619–637. https://doi.org/10.3144/expresspolymlett.2020.51

Saadiah, M. A., Nagao, Y., & Samsudin, A. S. (2021). Enhancement on protonation (H+) with incorporation of flexible ethylene carbonate in CMC–PVA–30 wt % NH4NO3 film. *International Journal of Hydrogen Energy*, *46*(33), 17231–17245. https://doi.org/10.1016/j.ijhydene.2021.02.187

Saadiah, M. A., & Samsudin, A. S. (2018). Study on ionic conduction of solid bio-polymer hybrid electrolytes based carboxymethyl cellulose (CMC)/polyvinyl alcohol (PVA) doped NH4NO3. *AIP Conference Proceedings*, *2030*(Cmc). https://doi.org/10.1063/1.5066864

Sallal, A. A., Hassan, H. M., & Ibrahim, M. (2022). Improving optical properties of polyvinyl alcohol (PVA) and carboxymethyl cellulose (CMC) as polymer blend films (CMC-PVA). *ACM International Conference Proceeding Series*, *Cmc*, 652–656. https://doi.org/10.1145/3584202.3584301

Shaikh, H. M., Anis, A., Poulose, A. M., Al-Zahrani, S. M., Madhar, N. A., Alhamidi, A., Aldeligan, S. H., & Alsubaie, F. S. (2022). Synthesis and Characterization of Cellulose Triacetate Obtained from Date Palm (Phoenix dactylifera L.) Trunk Mesh-Derived Cellulose. *Molecules*, *27*(4), 1–13. https://doi.org/10.3390/molecules27041434

Shamsuri, N. A., Zaine, S. N. A., Yusof, Y. M., Yahya, W. Z. N., & Shukur, M. F. (2020). Effect of

ammonium thiocyanate on ionic conductivity and thermal properties of polyvinyl alcohol–methylcellulose–based polymer electrolytes. *Ionics*, *26*(12), 6083–6093. https://doi.org/10.1007/s11581-020-03753-9

Shetty, S. K., Ismayil, Hegde, S., Ravindrachary, V., Sanjeev, G., Bhajantri, R. F., & Masti, S. P. (2021). Dielectric relaxations and ion transport study of NaCMC:$NaNO_3$ solid polymer electrolyte films. *Ionics*, *27*(6), 2509–2525. https://doi.org/10.1007/s11581-021-04023-y

Shukur, M. F., Hamsan, M. H., & Kadir, M. F. Z. (2018). Plasticized and plasticizer free lithium acetate doped polyvinyl alcohol-chitosan blend solid polymer electrolytes: Comparative studies. *Journal of Physics: Conference Series*, *1123*(1). https://doi.org/10.1088/1742-6596/1123/1/012001

Shyly, P. M., Ammakutti Sridevi, N., & Sumithraj Premkumar, P. (2022). Thermal and mechanical studies of nanochitosan incorporated polymethyl methacrylate-based composite electrolytes. *Journal of Engineering and Applied Science*, *69*(1), 1–14. https://doi.org/10.1186/s44147-022-00077-5

Singh, S. K., Dutta, D., & Singh, R. K. (2022). Polymer batteries. In *Polymers in Energy Conversion and Storage* (Issue October, pp. 197–216). CRC Press. https://doi.org/10.1201/9781003169727-10

Sohaimy, M. I. H., Zainuddin, N. I., & Isa, M. I. N. (2022). Plasticized CMC-ammonium acetate based solid biopolymer electrolyte: Ionic conductivity and transport study. *Journal of Sustainability Science and Management*, *17*(5), 139–148. https://doi.org/10.46754/jssm.2022.05.011

Stivala, S. S., & Reich, L. (1980). Structure vs stability in polymer degradation. *Polymer Engineering & Science*, *20*(10), 654–661. https://doi.org/10.1002/pen.760201003

Tan, X., Wu, Y., Tang, W., Song, S., Yao, J., Wen, Z., Lu, L., Savilov, S. V, Hu, N., & Molenda, J. (2020). Preparation of Nanocomposite Polymer Electrolyte via In Situ Synthesis of SiO_2 Nanoparticles in PEO. *Nanomaterials. 10*(1):157. https://doi:10.3390/nano10010157.

Tomić, N. Z. (2019). *Thermal studies of compatibilized polymer blends. Compatibilization of Polymer Blends: Micro and Nano Scale Phase Morphologies, Interphase Characterization, and Properties,* 489–510. https://doi.org/10.1016/B978-0-12-816006-0.00017-7

Triandani, N. W. P., Ndruru, S. T. C. L., Dharmi, N. K. H., Rochliadi, A., & Arcana, I. M. (2023). Preparation and characterization of shrimp shell waste derived carboxymethyl chitosan solid polymer electrolyte membrane. *Biomass Conversion and Biorefinery*, *14*(0123456789), 1–19. https://doi.org/10.1007/s13399-023-04632-9

Xi, G., Xiao, M., Wang, S., Han, D., Li, Y., & Meng, Y. (2021). Polymer-based solid electrolytes: material selection, design, and application. *Advanced Functional Materials*, *31*(9). https://doi.org/10.1002/adfm.202007598

Xiong, M., Tang, H., Wang, Y., & Pan, M. (2014). Ethylcellulose-coated polyolefin separators for lithium-ion batteries with improved safety performance. *Carbohydrate Polymers*, *101*(1), 1140–1146. https://doi.org/10.1016/j.carbpol.2013.10.073

Yang, T., Zheng, J., Cheng, Q., Hu, Y. Y., & Chan, C. K. (2017). Composite polymer electrolytes with Li7La3Zr2O12 garnet-type nanowires as ceramic fillers: mechanism of conductivity enhancement and role of doping and morphology. *ACS Applied Materials and Interfaces*, *9*(26), 21773–21780. https://doi.org/10.1021/acsami.7b03806

Yazie, N., Worku, D., Gabbiye, N., Alemayehu, A., Getahun, Z., & Dagnew, M. (2023). Development of polymer blend electrolytes for battery systems : recent progress , challenges , and future outlook. *Materials for Renewable and Sustainable Energy*, *0123456789*. https://doi.org/10.1007/s40243-023-00231-w

Zhang, J., Zhao, J., Yue, L., Wang, Q., Chai, J., Liu, Z., Zhou, X., Li, H., Guo, Y., Cui, G., & Chen, L. (2015). Safety-reinforced poly(propylene carbonate)-based all-solid-state polymer electrolyte for ambient-temperature solid polymer lithium batteries. *Advanced Energy Materials*, *5*(24), 1–10. https://doi.org/10.1002/aenm.201501082

Zhang, X., Liu, T., Zhang, S., Huang, X., Xu, B., Lin, Y., Xu, B., Li, L., Nan, C. W., & Shen, Y. (2017). Synergistic coupling between Li6.75La3Zr175Ta0.25O12 and poly(vinylidene fluoride) induces high ionic conductivity, mechanical strength, and thermal stability of solid composite electrolytes. *Journal of the American Chemical Society*, *139*(39), 13779–13785. https://doi.org/10.1021/jacs.7b06364

Zulkifli, A., Saadiah, M. A., Mazuki, N. F., & Samsudin, A. S. (2020). Characterization of an amorphous materials hybrid polymer electrolyte based on a $LiNO_3$-doped, CMC-PVA blend for application in an electrical double layer capacitor. *Materials Chemistry and Physics*, *253*, 1–58.